Electronic Supplementary Material (ESI) for RSC Advances.

Electronic Supplementary Information

Interface metallization enabled ultra-Stable Fe_2O_3 hierarchical anode for pseudocapacitors

Songyang Su[†, a], Lu Shi[†, a], Wentao Yao[†, a], Yang Wang[b], Peichao Zou[a], Kangwei Liu[a], Min Wang[a], Feiyu Kang[c], and Cheng Yang[*, a]

[a] Division of Energy and Environment, International Graduate School at Shenzhen, Tsinghua University, Shenzhen 518055, China
[b] State Key Laboratory of Electronic Thin Films and Integrated Devices, School of Optoelectronic Information, University of Electronic Science and Technology of China (UESTC), Chengdu 610054, P. R. China
[c] School of Materials Science and Engineering, Tsinghua University, Beijing 100084, China

[†] These authors contributed equally to this work.

*Corresponding author e-mail address: yang.cheng@sz.tsinghua.edu.cn.

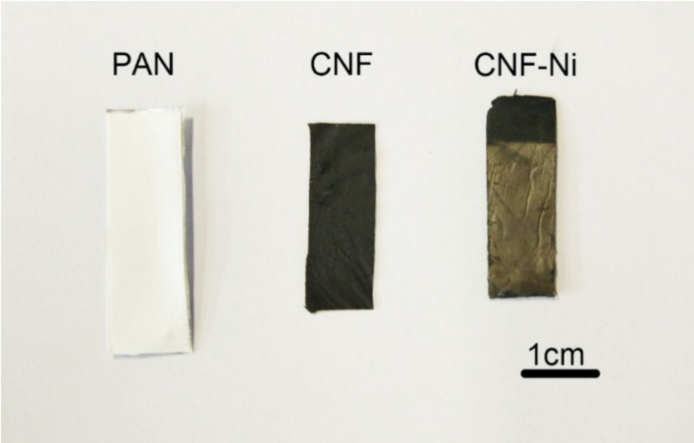

Figure S1 Optical photos of PAN, CNF and CNF-Ni films, respectively.

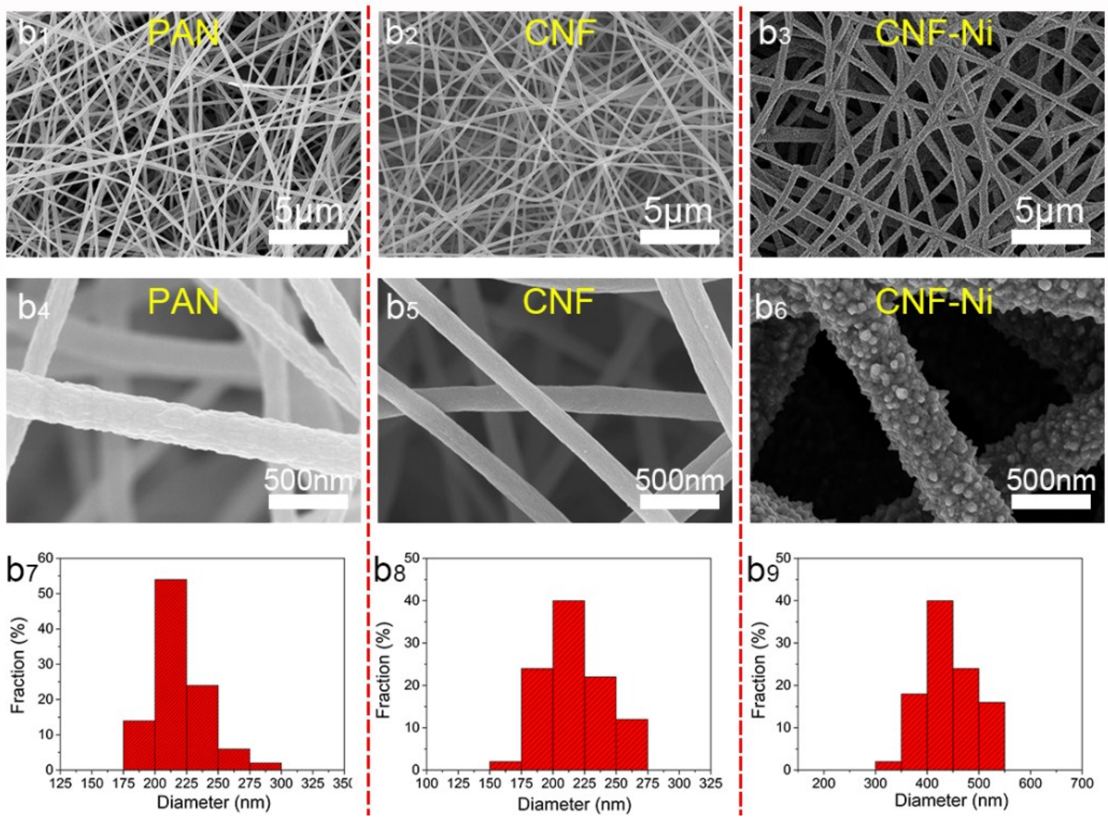

Figure S2 SEM images of the fibers film: b_{1-3}) SEM images of PAN, CNF, and CNF-Ni, respectively; b_{4-6}) their enlarged SEM images, respectively; b_{7-9}) their diameter distribution graphs, respectively.

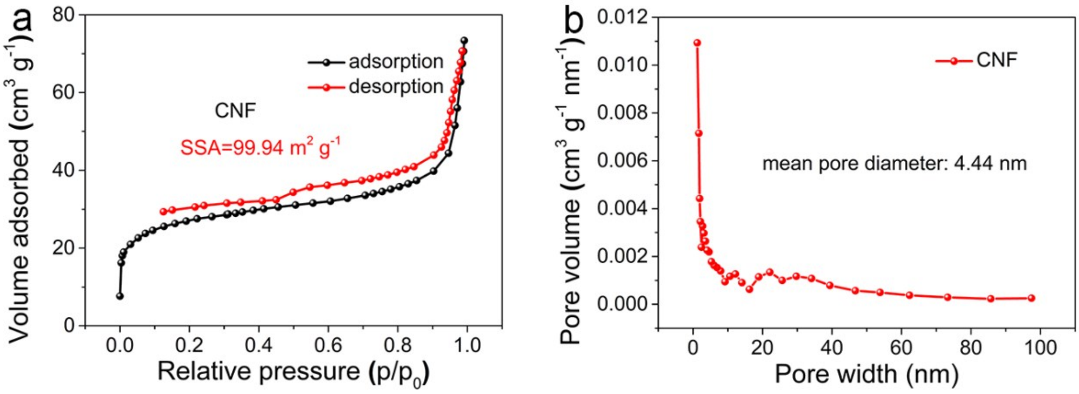

Figure S3 (a) Adsorption isotherm curves of the CNF films. The SSAs are calculated as 99.94 m^2 g^{-1}. (b) BJH pore size distribution plot of the CNF film, its pore size distribution is in the range of 1 - 10 nm with an average pore size of 4.44 nm.

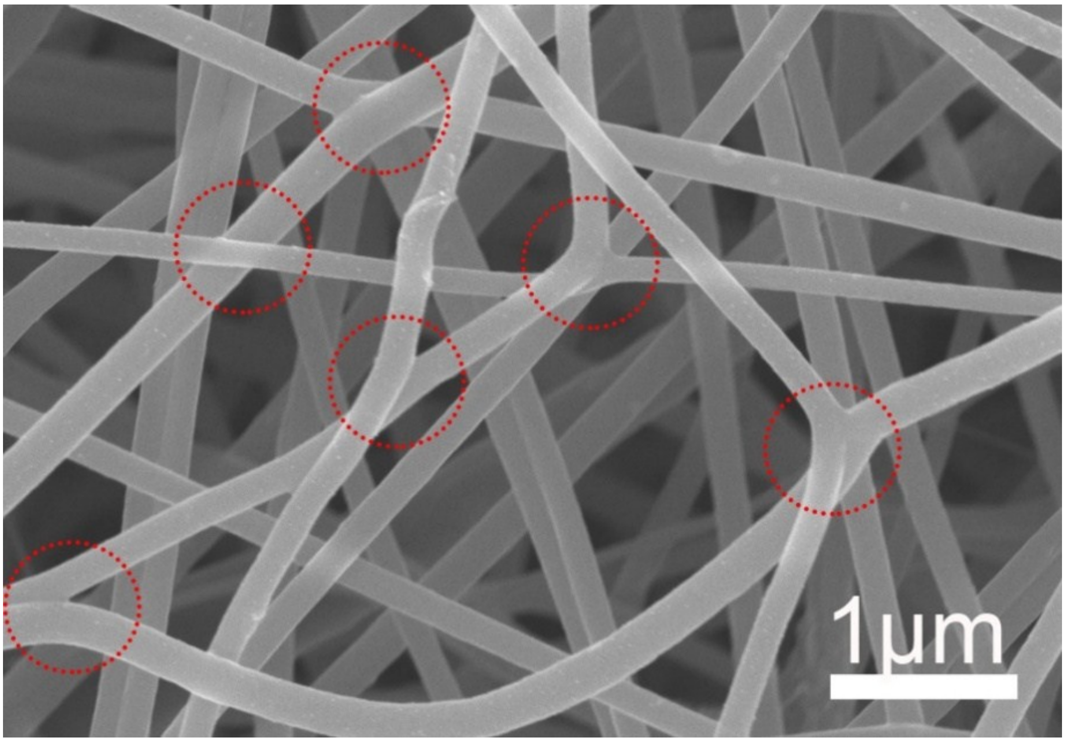

Figure S4 Crosslinked phenomena of CNFs, which could significantly reduce the contact resistance of the whole film.

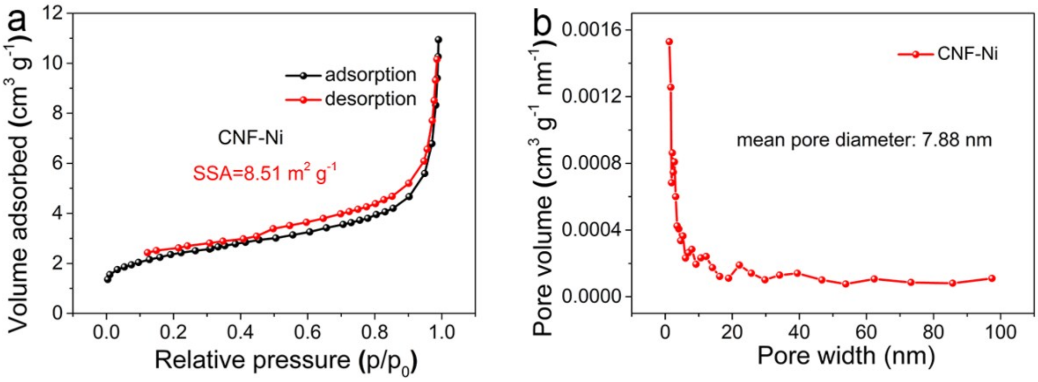

Figure S5 (a) Adsorption isotherm curves of the CNF-Ni films. The SSAs are calculated as 8.51 m^2 g^{-1}. (b) BJH pore size distribution plot of the CNF-Ni film, its pore size distribution is in the range of 1 - 10 nm with an average pore size of 7.88 nm.

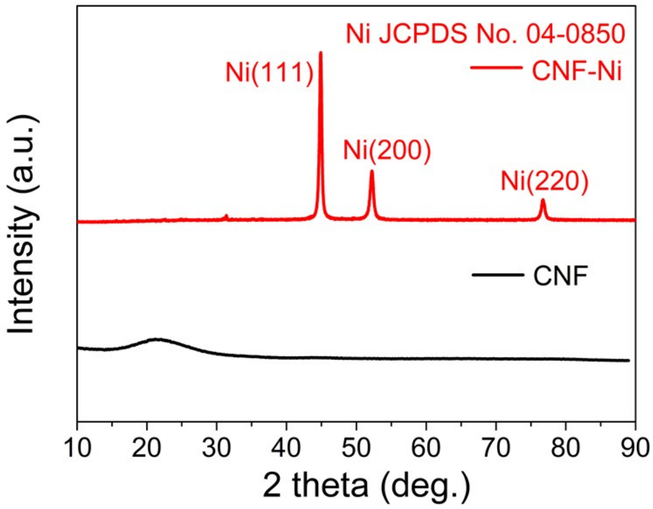

Figure S6 XRD spectra comparison of CNF and CNF-Ni films.

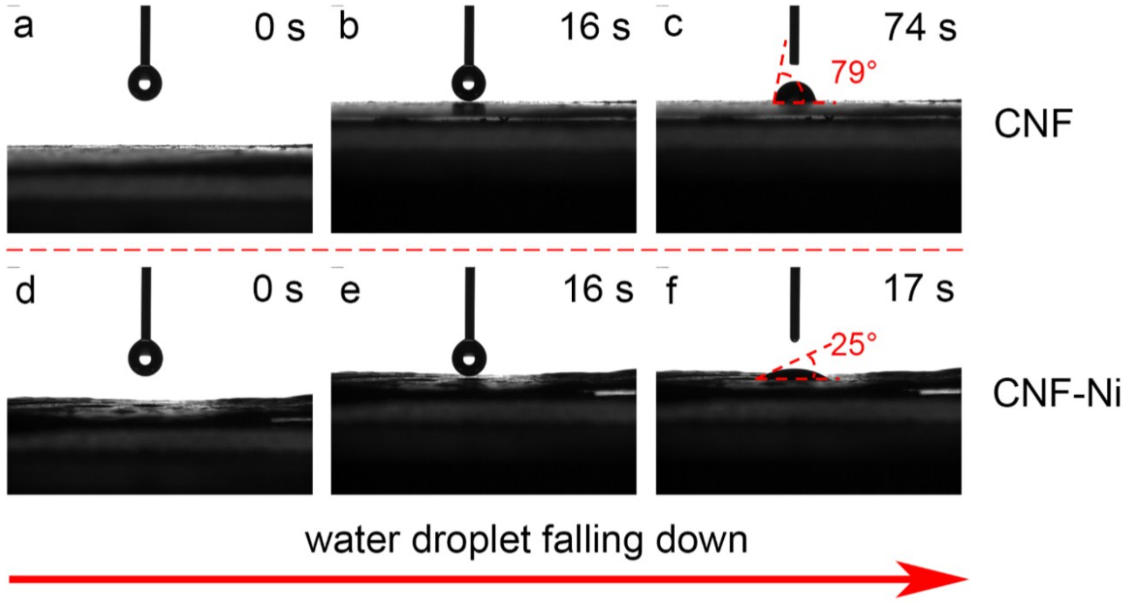

Figure S7 Water contact angle measurement of the CNF and CNF-Ni surface. From (b) to (c), the time span is within 58 seconds. From (e) to (f), the time span is within 1 second. The contact angles of CNF film and CNF-Ni film indicated the CNF-Ni-based electrodes are super hydrophilic.

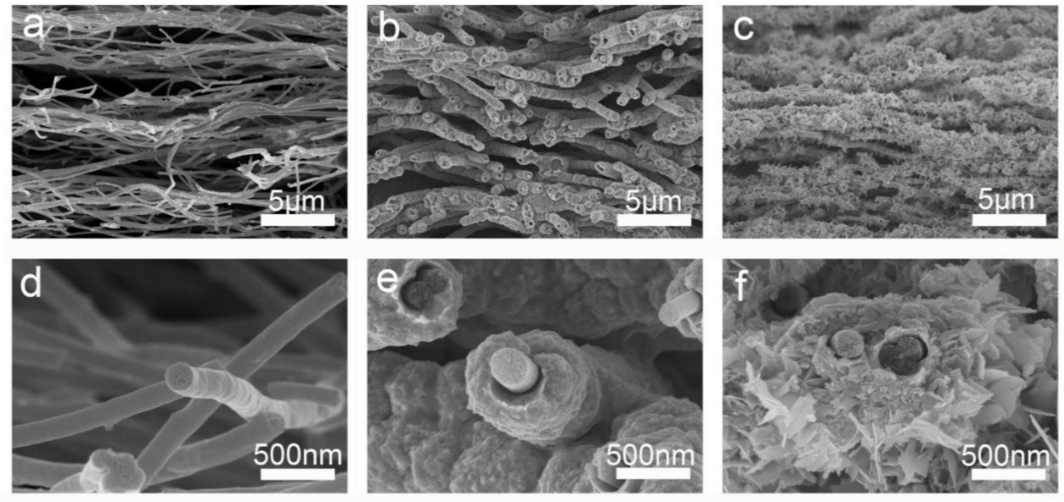

Figure S8 (a-c) Cross-sectional SEM images of the CNF, CNF-Ni and CNF-Ni@Fe_2O_3 films, respectively. (d-f) Their enlarged SEM images, respectively.

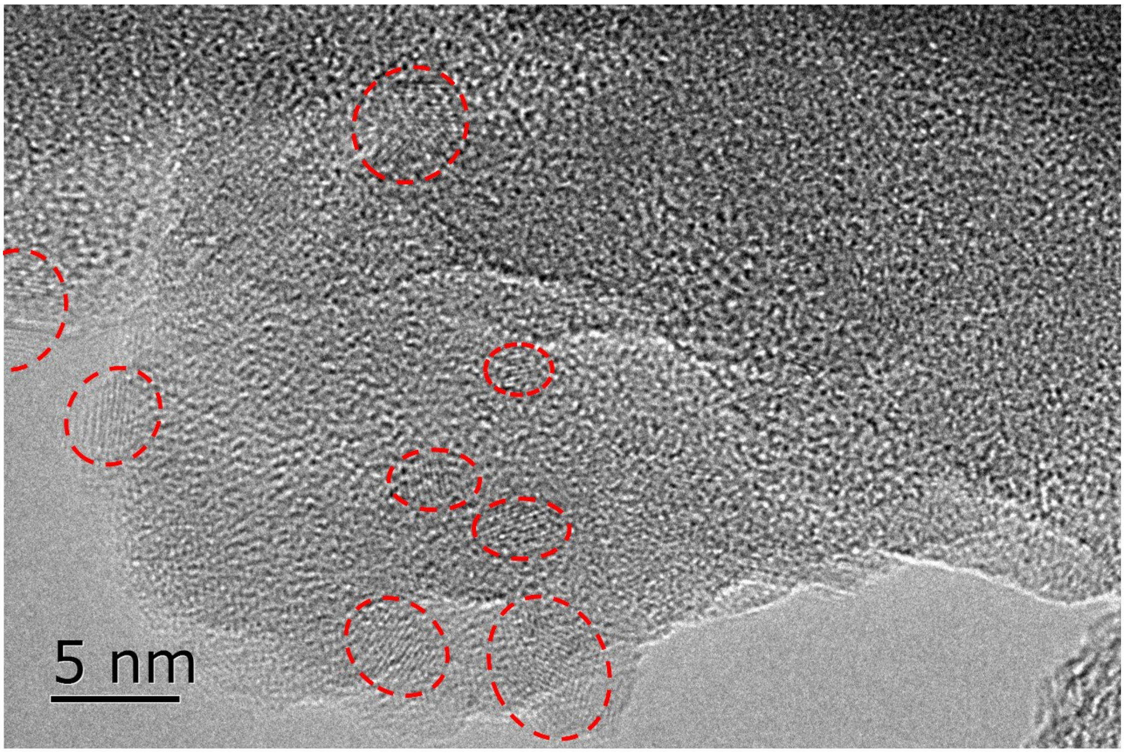

Figure S9 HR-TEM image of the 2D Fe_2O_3 suggests that the crystalline in the amorphous heterogeneous structure of Fe_2O_3.

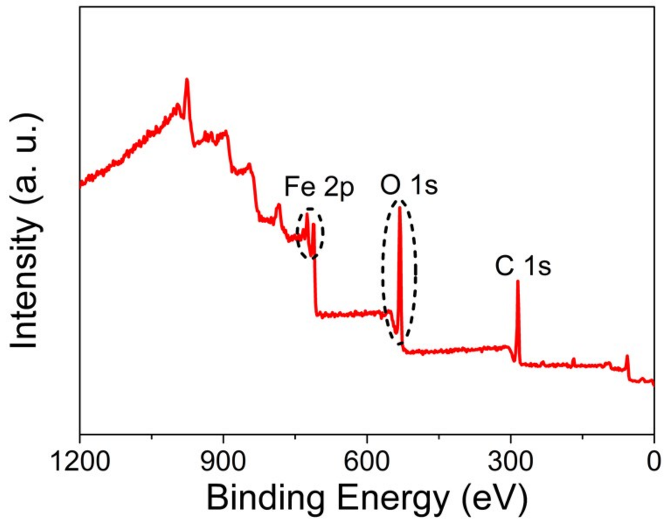

Figure S10 XPS full spectrum of the 2D Fe_2O_3, the C 1s signal at 284.6 eV is used as the reference. The peaks in the range of 740 - 700 eV and 535 - 525 eV are assignable to the Fe 2p and O 1s spectra, respectively.

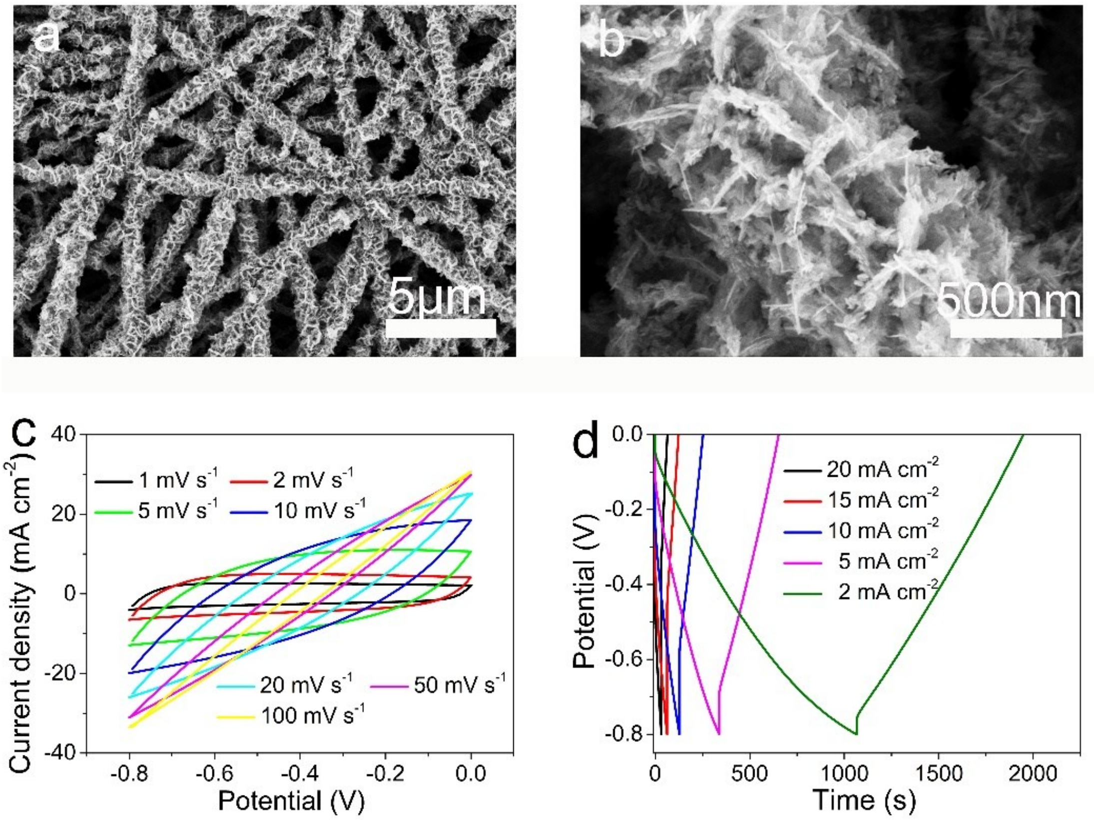

Figure S11 (a, b) SEM images of the CNF@Fe_2O_3 electrode. Electrochemical performance of the CNF@Fe_2O_3 electrode. (c) CV curves at the scan rates ranging from 1 mV s^{-1} to 100 mV s^{-1}; (d) GCD curves at current densities range of 2 - 20 mA cm^{-2}.

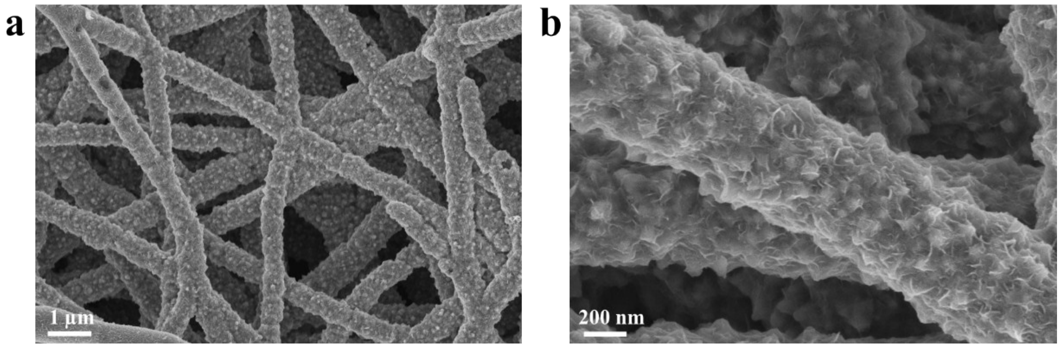

Figure S12 SEM images of the CNF-Ni@Fe_2O_3 film after cycling.

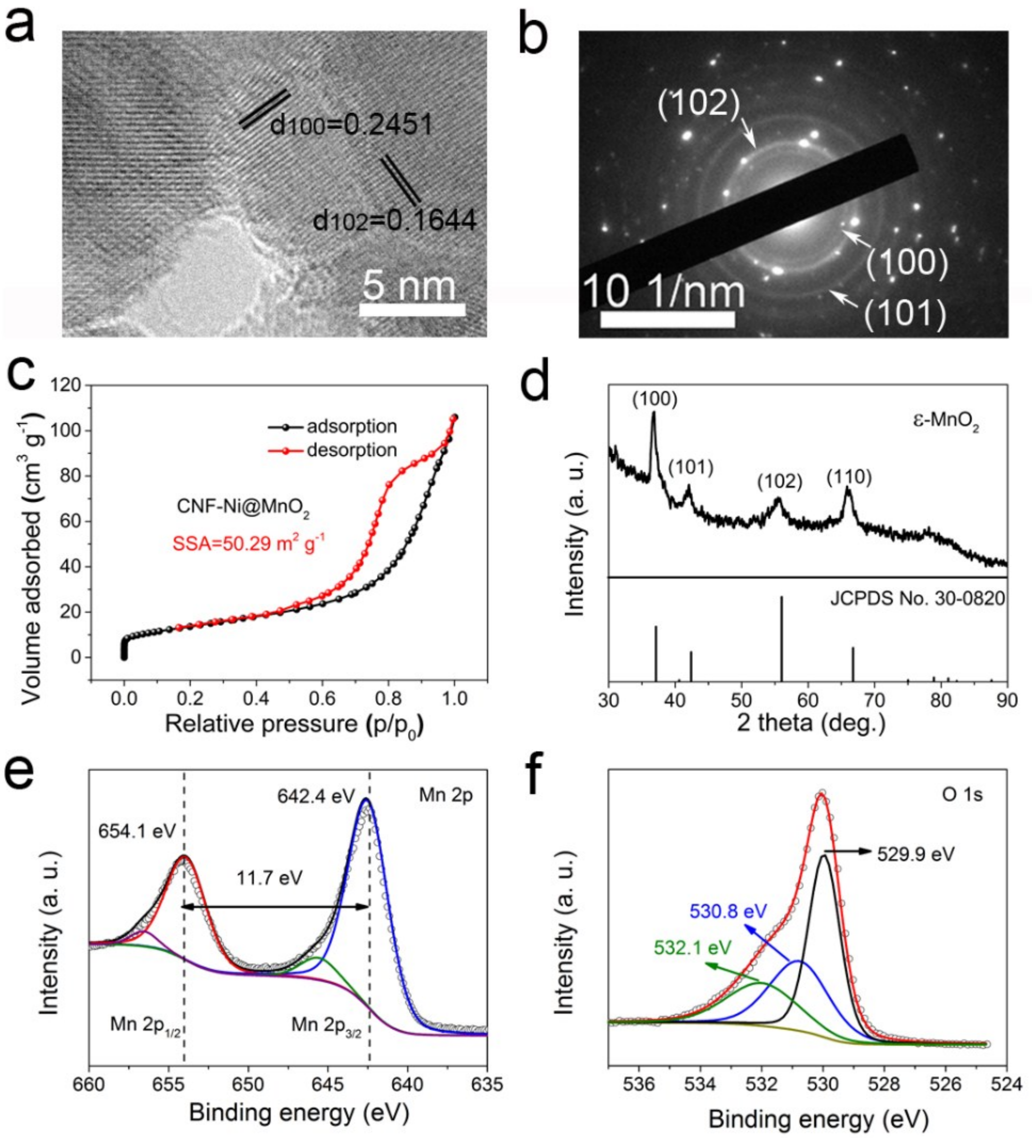

Figure S13 (a) HR-TEM image and (b) SEAD pattern of MnO_2; (c) Adsorption isotherm curve of the CNF-Ni@MnO_2 film; (d) XRD spectrum of MnO_2; (e), (f) HR-XPS spectra of Mn 2p and O 1s, respectively.

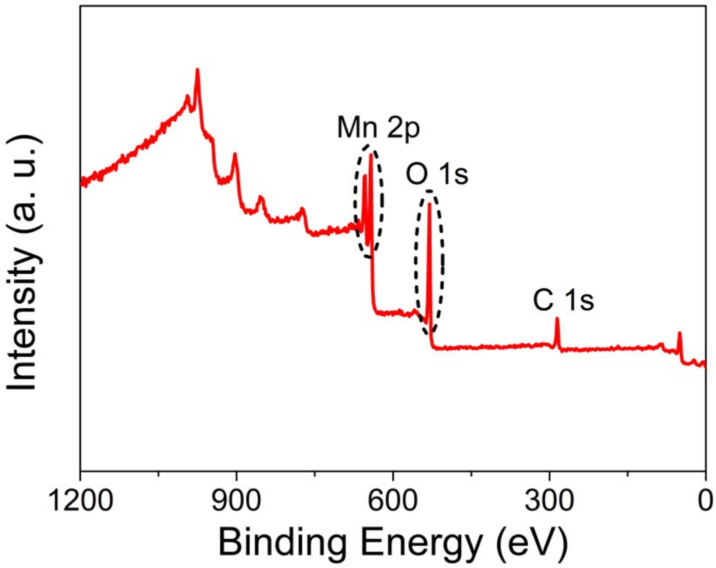

Figure S14 XPS full spectrum of the 2D MnO_2. The C 1s signal at 284.6 eV is used as the reference to calibrate the binding energies of Mn and O. The peaks in the range of 660 - 630 eV and 540 - 520 eV are assignable to the Mn 2p and O 1s spectra, respectively.

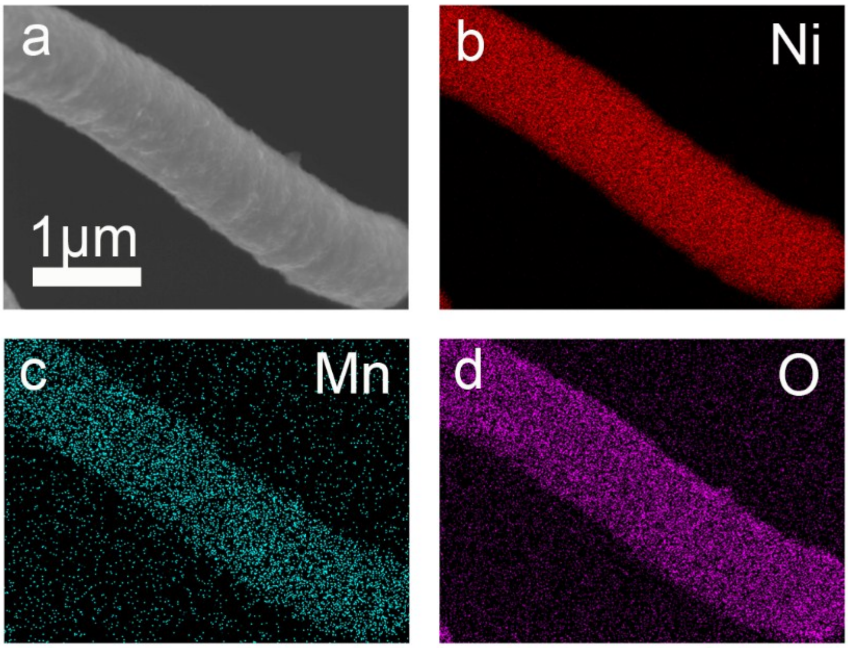

Figure S15 SEM image (a) of CNF-Ni@MnO_2 fiber combined with energy-dispersive spectroscopy (EDS) mapping in the same area and relative intensities of (b) C, (c) Ni, (d) Mn and (e) O elements, showing that these elements are distributed evenly over the fibers.

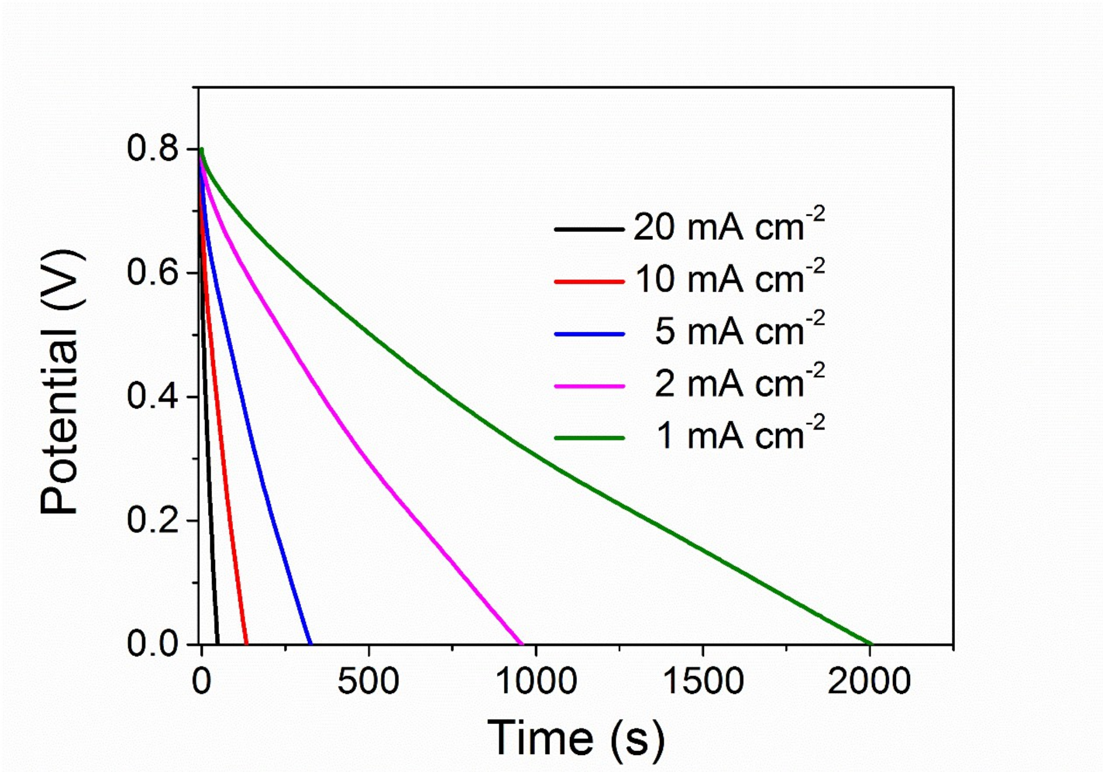

Figure S16 GCD curves of the CNF-Ni@MnO_2 cathode at different current densities ranging from 1 to 20 mA cm^{-2}.

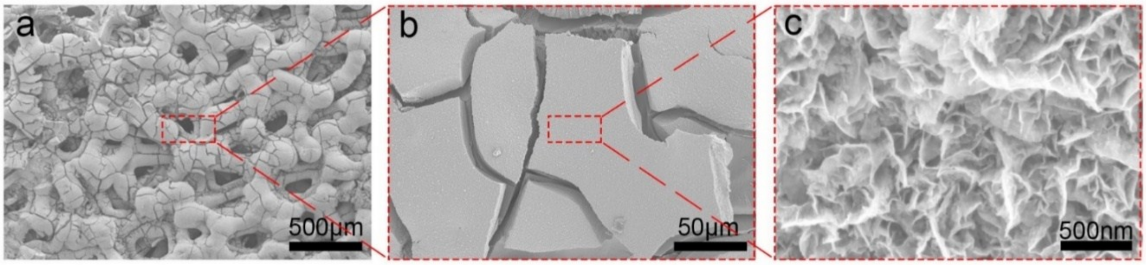

Figure S17 (a-c) SEM images of $NF@MnO_2$ at different magnifications. Cracks can be clearly found on the $NF@MnO_2$ sample surface.

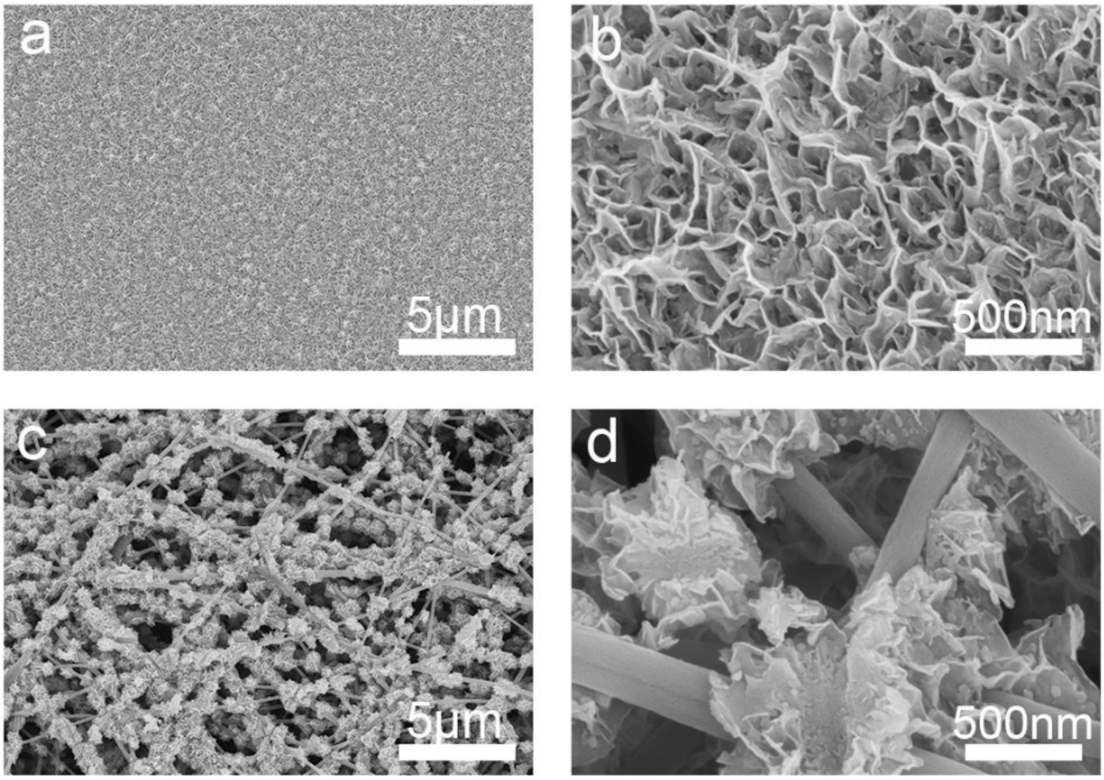

Figure S18 SEM images of CNF@MnO_2 at different magnifications. (a), (b) The outer part of CNF@MnO_2 sample; (c), (d) the inner part of CNF@MnO_2 sample.

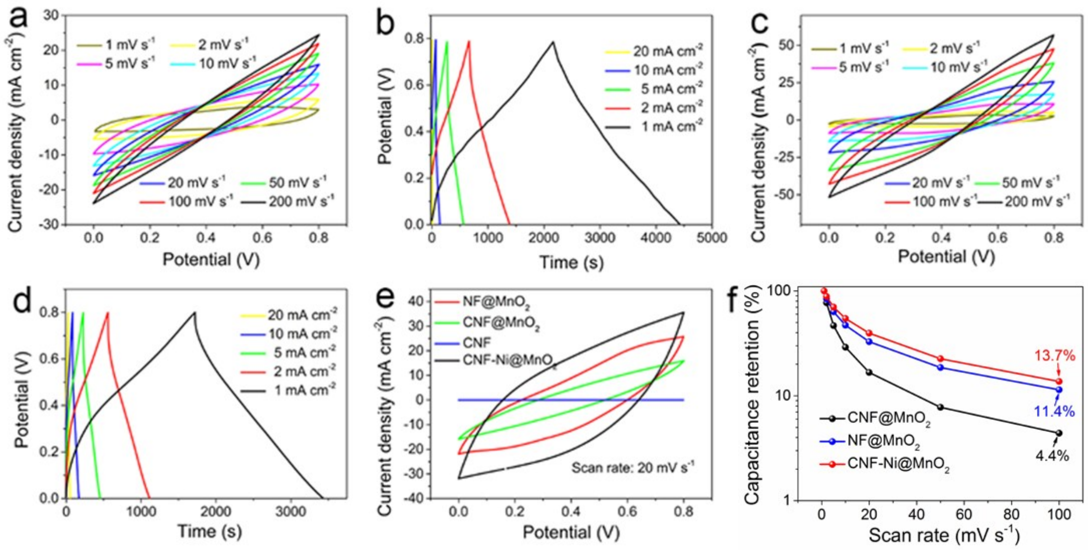

Figure S19 Electrochemical performance of the CNF@MnO_2 and NF@MnO_2 electrodes. (a) CV curves of CNF@MnO_2 at scan rates of 1 – 200 mV s^{-1}; (b) GCD curves of CNF@MnO_2 at current densities ranging from 1 to 20 mA cm^{-2}; (c) CV curves of NF@MnO_2 at scan rates of 1 – 200 mV s^{-1}; (d) GCD curves of NF@MnO_2 at current densities ranging from 1 to 20 mA cm^{-2}; (e) CV curves of CNF film, CNF@MnO_2, NF@MnO_2 and CNF-Ni@MnO_2 with the same mass loading at 20 mV s^{-1} in 0.5 M Na_2SO_4 electrolyte. The almost negligible CV area of CNF film indicates MnO_2 contribute to most of the capacitance. The larger CV area of CNF-Ni@MnO_2 compared with that of CNF@MnO_2 and NF@MnO_2 demonstrate the higher specific capacitance as the result of conductive scaffold; (f) the capacitance retention versus scan rate with the same mass loading for NF@MnO_2, CNF@MnO_2, and CNF-Ni@MnO_2 electrodes.

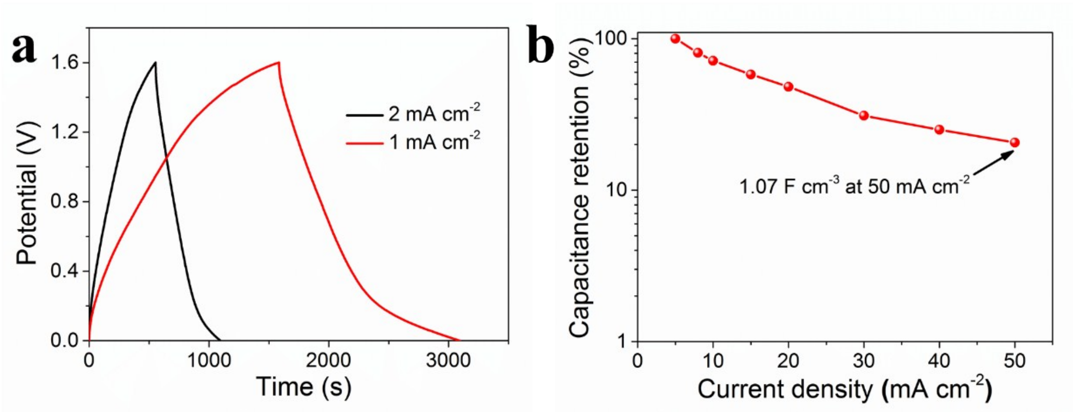

Fig. S20 (a) GCD curves at current densities of 1 and 2 mA cm^{-2}; (b) Capacitance retention value versus current density calculated by GCD curves.

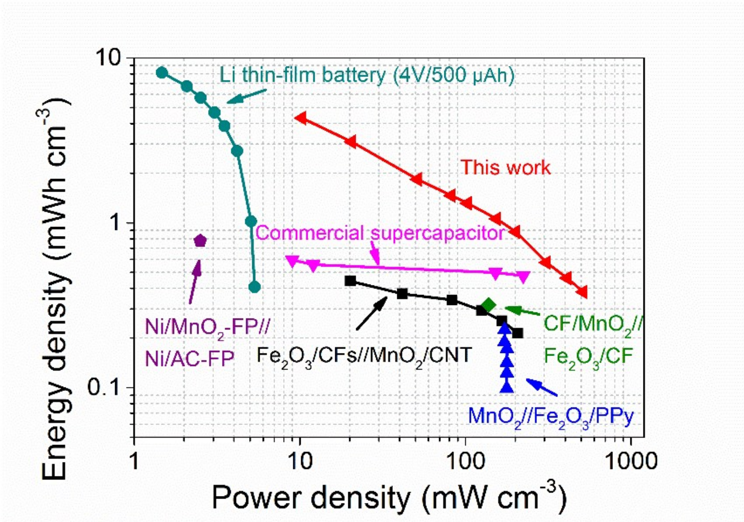

Fig. S21 Ragone plot of our supercapacitor as compared to other recently-reported ones.

Table S1. A comparison of electrochemical properties among some of the recently reported supercapacitors with our work

Supercapacitors	Areal capacitance ($F \cdot cm^{-2}$)	Volumetric capacitance ($F \cdot cm^{-3}$)	Power density ($mW \cdot cm^{-3}$)	Energy density ($mWh \cdot cm^{-3}$)	Ref.
Fe_2O_3/CFs//MnO_2/CNT	/	0.67	208	0.44	[1]
Fe_2O_3-P//MnO_2	/	/	258	0.42	[2]
RuO_2//Fe_2O_3	0.06	4.9	9.1	1.5	[3]
α-Fe_2O_3/C/α-Fe_2O_3/MnO_x	/	1.28	155	0.64	[4]
MnO_2//Fe_2O_3/PPy	/	0.84	166	0.22	[5]
Ag-NW/PEDOT:PSS-NP//MnO_2	/	4.64	369	0.41	[6]
rGO/CNT//rGO/CNT	0.33	2	800	1.7	[7]
Co_9S_8/CC//Co_3O_4@RuO_2/CC	0.34	3.42	890	1.44	[8]
CNF-Ni@MnO_2//CNF-Ni@Fe_2O_3	0.94	12.15	515	4.32	This work

References

1. Y. Li, J. Xu, T. Feng, Q. Yao, J. Xie, and H. Xia, Advanced Functional Materials, 2017, 27, 1606728.
2. H. Liang, C. Xia, A.-H. Emwas, D. H. Anjum, X. Miao, and H. N. Alshareef, Nano Energy, 2018, 49, 155-162.
3. J. Y. Seok, J. Lee, and M. Yang, ACS Appl Mater Interfaces, 2018, 10, 17223-17231.
4. D. Sarkar, S. Pal, S. Mandal, A. Shukla, and D. D. Sarma, Journal of The Electrochemical Society, 2017, 164, A2707-A2715.
5. L. Wang, H. Yang, X. Liu, R. Zeng, M. Li, Y. Huang and X. Hu, Angew Chem Int Ed Engl, 2017, 56, 1105-1110.
6. Y. Zeng, Y. Han, Y. Zhao, Y. Zeng, M. Yu, Y. Liu, H. Tang, Y. Tong and X. Lu, Advanced Energy Materials, 2015, 5, 1402176.
7. X. Lu, Y. Zeng, M. Yu, T. Zhai, C. Liang, S. Xie, M. S. Balogun and Y. Tong, Adv Mater, 2014, 26, 3148-3155.
8. X. Tang, R. Jia, T. Zhai, and H. Xia, ACS Appl Mater Interfaces, 2015, 7, 27518-27525.
9. S. Yang, X. Song, P. Zhang, and L. Gao, ACS Appl Mater Interfaces, 2015, 7, 75-79.